Sensors and Materials, Vol. 36, No. 9 (2024) 3797–3815
MYU Tokyo

S & M 3768

On-machine Fabrication of Boron-doped Polycrystalline Diamond Cutting Tools by Combining Wire Electrical Discharge Machining and Abrasive Grinding

Yue-Feng Lin,* Pei-Yu Lai, and Yuan-Xiu Luo

Department of Mechanical Engineering, National Chin-Yi University of Technology,
No. 57, Sec. 2, Zhongshan Rd., Taiping Dist., Taichung 411030, Taiwan (R.O.C.)

(Received April 30, 2024; accepted July 18, 2024)

Keywords: boron-doped polycrystalline diamond, microcutting tool, wire-EDM, abrasive grinding, cutting edge, CCD

A sequential technique that combines wire electrical discharge machining (wire-EDM) and abrasive grinding on dedicated equipment improves the edge quality of boron-doped polycrystalline diamond (BD-PCD) cutting tools. In this study, we focus on material removal mechanisms during BD-PCD machining and surface graphitization caused by wire-EDM thermal damage. Surface topography is used to distinguish ductile- and brittle-regime grinding in tool production. Resin-bonded diamond wheels outperform electroplated diamond wheels in abrasive grinding owing to their self-sharpening capabilities. The experimental results show that BD-PCD tools have higher mechanical properties and performance than standard PCD tools. Maximum edge chipping on BD-PCD surfaces depends on the depth of cut and grinding speed. Microgrinding experiments on BK7 glass reveal that the recommended tool manufacturing approach, which merges wire-EDM and abrasive grinding, results in high-quality surfaces free of microcracks and achieves a surface roughness of 6 nm Sa. Abrasion on the flank face and chipping on the periphery are the main wear patterns on grinding tools. In this study, we improve our understanding of BD-PCD microcutter production, focusing on parameter management for optimal surface quality, edge integrity, and tool performance. We emphasize the necessity of choosing the right grinding wheel to achieve the necessary surface and subsurface quality when making microcutting tools. Raman spectroscopy results are used to explain thermal deterioration when diamond grains turn into graphite at high manufacturing temperatures. We address the challenges of producing high-quality microcutting tools and offer insights into improving BD-PCD tool performance and edge quality.

1. Introduction

The production of optical components is a priority in the manufacturing industry, with a focus on the development of cutting tools that have both high performance and long life.(1) Achieving high accuracy and precision is imperative in the grinding of optical components. The

*Corresponding author: e-mail: yflin@ncut.edu.tw
https://doi.org/10.18494/SAM5097

ISSN 0914-4935
https://myukk.org/

challenges have prompted the exploration of boron-doped polycrystalline diamond (BD-PCD) as a potential solution.[2–4] BD-PCD, also called electrically conductive PCD, has emerged as a promising material for cutting tools. In contrast to standard PCD (S-PCD), BD-PCD exhibits higher electrical conductivity while still being fabricated using identical techniques as for conventional PCD, as reported in Ref. 5. BD-PCD exhibits lower specific resistance and thermal conductivity than S-PCD, showcasing its innovativeness. Notably, their exceptional wear resistance and chemical stability are emphasized as crucial qualities that improve their performance and durability as cutting tools. Despite their many advantages, producing BD-PCD cutting tools poses a significant challenge. BD-PCD hardness and wear resistance are the primary factors contributing to the difficulties of BD-PCD.[3,5] Numerous academic experts and investigators have dedicated their efforts to formulating innovative fabrication approaches to enhance the efficacy of BD-PCD microcutting tools. Among the various fabrication technologies available, the most commonly utilized ones include abrasive grinding with diamond wheels, techniques based on electrical discharge machining (EDM), laser beam machining, and wire-EDM.[6,7] To improve the fabrication of BD-PCD cutting tools, on-machine fabrication techniques have also been developed.[8] Despite this, the on-machine fabrication process presents several obstacles. The most significant barriers are related to the complexity of the manufacturing procedure and the precise machining required to achieve the desired tool geometry and surface finish. In this research, we employ a sequential integration of wire-EDM and abrasive grinding techniques on a newly developed machine tool to achieve the sharpening and finishing of the cutting edges of BD-PCD microtools. The aforementioned machine tool has been specifically designed to carry out on-machine tool fabrication and metrology tasks, with the added benefit of minimizing issues related to tool handling, reclamping errors, and repositioning errors.

The appeal of EDM as a method for fabricating microcutting tools is ascribed to its noncontact nature and its capacity to eliminate materials regardless of material hardness. Multiple research studies have revealed that BD-PCD can be successfully machined by employing wire-EDM methods.[9–11] To manufacture PCD microend mills with particular shapes, Cheng *et al.* used a specialized ultraprecision machine tool with a unique six-axis wire-EDM tool fabrication system.[12] They also reported using the finite element method to fabricate and analyze PCD micro–straight edge microend mills with a negative rake angle by wire-EDM.[13] In contemporary times, multiprocessing manufacturing methods have emerged for fabricating BD-PCD microcutting tools. These techniques involve the utilization of at least two distinct machining technologies in a sequential manner across different machine tools.[14] Morgan *et al.* suggested a hybrid fabrication approach that combines wire-EDM, wire electrical discharge grinding, and micro-EDM techniques to create microtools suitable for milling grooves in soda-lime glass and pockets in ultralow-expansion glass.[15] In the context of micromachining, Oliaei *et al.* noted that the use of microend mills has been favored, particularly for processing silicon wafers and tungsten carbide materials. PCD microend mills with hexagonal tool geometry and a significant negative rake angle at the bottom of the tool were created using a highly accurate micro–wire-EDM machine with a rotary indexing table.[6] According to such earlier works, wire-EDM has been identified as a practical machining technique that can be sequentially combined with other machining methodologies to produce BD-PCD microcutting tools.

Abrasive grinding using diamond wheels is widely employed in the manufacturing industry to produce microcutting tools using various tool materials.[10,11,16,17] The grinding parameters for making PCD micromill tools were investigated using the Taguchi method.[18] The grinding performance of the PCD compact was primarily affected by the grain size of the PCD compact itself, as evidenced by experimental results. Subsequently, the grain size of the abrasive wheel, feed rate, and grinding speed were identified as additional factors impacting the grinding performance. Despite the apparent limitations posed by size restrictions, significant grinding wheel wear, and a relatively low material removal rate, it is important to acknowledge the relevance of abrasive grinding in the fabrication of microcutting tools characterized by small diameters and intricate geometries.[18] The use of abrasive grinding in the manufacturing of BD-PCD cutting tools continues to offer distinct benefits. Zhan *et al.* found that wire-EDM generates an edge with an EDM metamorphic layer, which has been observed to reduce the strength of the resulting edge substantially.[18] The application of precision abrasive grinding is highly advantageous in manufacturing microcutting tools. According to Li *et al.*, it is likely that the compressive residual stress was released during the abrasive grinding, as the stress of ground PCD tools was found to be lower than that of raw PCD.[19] The instability of the PCD structure becomes apparent when PCD is subjected to elevated residual stress levels. The utilization of an abrasive grinding process can produce durable finishing tools through the release of residual stress. Previous research has demonstrated the potential application of abrasive grinding in creating BD-PCD cutting tools.

Despite considerable research on glass grinding using commercial diamond grinding wheels, further research on using commercial diamond grinding wheels for BD-PCD rod grinding is still needed. In this study, a tool manufacturing system was developed to address concerns related to tool handling problems, such as reclaiming and repositioning errors. Experiments were conducted to examine the impact of the cutting depth and grinding speed on the maximum edges and surfaces of BD-PCD microcutters, and the best grinding parameters for the production of microtools were determined. In this study, a set of microgrinding experiments were conducted on BK7 glass to assess the effectiveness of the proposed tool manufacturing method. Three distinct cutting tools were developed through wire-EDM, sequential wire-EDM in conjunction with abrasive grinding employing electroplated diamond wheels, and sequential wire-EDM combined with abrasive grinding utilizing resin-bound diamond wheels. In addition, the material removal mechanisms in the sequential manufacturing procedures for wire-EDM and abrasive grinding were also presented. In this study, we aim to improve the edge quality of BD-PCD cutting tools by sequentially combining wire-EDM and abrasive grinding on a single machine.

2. Experimental Equipment and Methods

2.1 Machine equipment design and assembly

A tabletop machining tool specifically focused on wire-EDM and abrasive grinding operations was carefully designed and built. This tool, depicted in Fig. 1, is aimed at improving and refining the cutting edge of ultrahard microcutting tools. Moreover, this particular machine

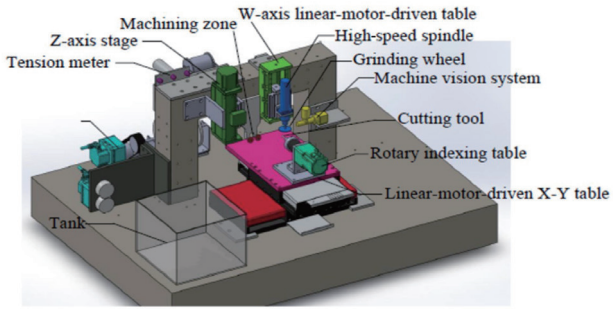

(a)

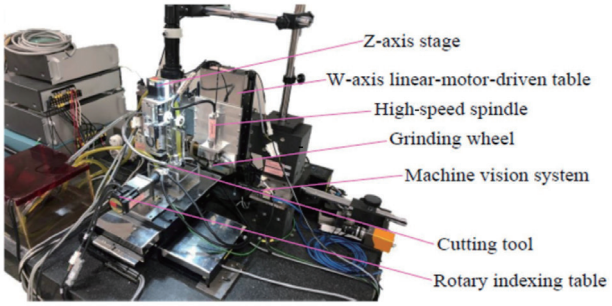

(b)

Fig. 1. (Color online) Specially designed tabletop machine tool for fabricating microcutting tools. (a) Overall machine design. (b) Photo of developed machine tool.

tool is capable of on-site evaluation of tool geometries. The machine tool comprises many components, including a gantry-type mechanical framework, a five-axis motion control system, an oil-based isopulse generator, a computer numerical control (CNC) system, a wire transport system, and a machine-vision-based subsystem. The motivation for creating the isopulse DC generator stemmed from the aim of producing discharge current pulses that exhibit uniform discharge durations and peak current levels. The wire transport system, consisting of a wire electrode supply equipment and a wire feed control device, was implemented to guarantee continuous wire transport and uphold stable tension levels. As a feedback device, the wire tension management system utilized a HANS-SCHMIDT TS1-2000-A2-RS232-CE1 tension meter. Various capabilities, such as five-axis motion control, closed-loop wire tension management, and on-site machine-vision-based measurement, were integrated using an IMP2 motion control card and a remote input/output (I/O) card in the CNC system.

A rigorously built machine vision system was used to enable the precise assessment of the frontal and lateral aspects of cutting tool geometries. The system is composed of two monochrome cameras (BFLY-U3-13S2M-CS) utilizing CCD technology, together with two optical lenses (KCM-4D-65C) and two light sources. The resolution achieved by the device is a noteworthy 1.12 μm per pixel. This level of detail allows for accurate and direct measurements to be conducted. The machine is outfitted with four linear axes, labeled explicitly as *X*, *Y*, *Z*, and *W*, each with a precision of 0.1 μm. Furthermore, the system has a rotation axis denoted as B, which

exhibits an angular accuracy of 0.001°. A precisely built *XY* table, driven by a linear motor, was developed to provide accurate motion control and facilitate the operation of the rotary indexing table. When dealing with BD-PCD microtools equipped with a cross-shape cutting edge, the abrasive grinding method must ensure that the rake and flank faces are finished. A table powered by a linear motor was designed to achieve this objective. The table exhibits a resolution of 0.1 μm, allowing for a minimal depth of cut of 0.1 μm along the *W*-axis. This feature serves to reduce the likelihood of edge chipping or microcracking. The table, driven by a linear motor along the *W*-axis, was outfitted with a spindle that utilizes ceramic bearings to achieve a maximum spindle speed of 40000 rpm. This particular arrangement enabled the efficient implementation of abrasive grinding procedures. The high-speed spindle, produced by Nakanishi Inc. (Japan), demonstrates a spindle runout below 1 μm, satisfying the criteria for high-precision grinding. The machine tool was carefully positioned on top of a granite surface plate to achieve stability and provide a dependable reference point.

2.2 Manufacturing of BD-PCD microcutting tools

The primary objective of this study is to analyze the material removal process of BD-PCD microtools using an experimental design machine. Furthermore, we examine the impact of grinding parameters, namely, the depth of cut and grinding speed, on the edge integrity and surface quality of BD-PCD microcutting tools. Moreover, in this study, microtools are produced using three separate manufacturing procedures. Following this, the produced cutting tools are evaluated by performing microgrinding on optical glass. A designed and built BD-PCD microtool featuring a cross-shaped edge was made to suit the requirements of BK7 glass microgrinding. The primary emphasis was on attaining high cutting precision and efficient chip removal.

In the wire-cutting experiments, we utilized a copper wire of 100 μm diameter. A 70-mm-diameter workpiece was made of a polycrystalline composite doped with boron. This composite material was made of a tungsten carbide matrix, which was further stabilized by a cobalt binding layer and a diamond phase with particles of 5 μm diameter. The tool materials utilized in this study were S-PCD and BD-PCD to facilitate comparative analysis. The mechanical properties of these materials are shown in Table 1. The composition of BD-PCD was characterized by a diamond content of 92 wt% and a cobalt content of 8 wt%.

Figure 2 shows a schematic of the production method employed for BD-PCD tools. The production of BD-PCD cutting tools comprises four separate steps. The BD-PCD composite workpiece is initially segmented into smaller circular forms via a commercially accessible wire-cut machine, JSEDM Model W-A30. Each circular chip produced exhibits a diameter of 1 mm. Following that, the BD-PCD chip is carefully attached to the carbide tool holder by silver welding performed by Taiwan Baishida Industrial Co., Ltd. The instrument utilized in this investigation is an inflexible metallic rod of 28 mm length. Subsequently, the BD-PCD cutting tools undergo wire-EDM operations employing a specifically designed machine tool to obtain accurate and precise dimensions. The enhancement of tool quality can be achieved using abrasive grinding procedures on the same machine, utilizing two distinct types of diamond

Table 1
Mechanical properties of S-PCD and BD-PCD materials.

Material property	S-PCD	BD-PCD
Young's modulus (Gpa)	900	800–870
Hardness, Knoop (KH) (Gpa)	50	50–70
Fracture toughness (MPa$\sqrt{m}$)	6.55	8.89
Thermal conductivity (W/m·K)	560	440–580
Density (g/cm^3)	3.85	4.1

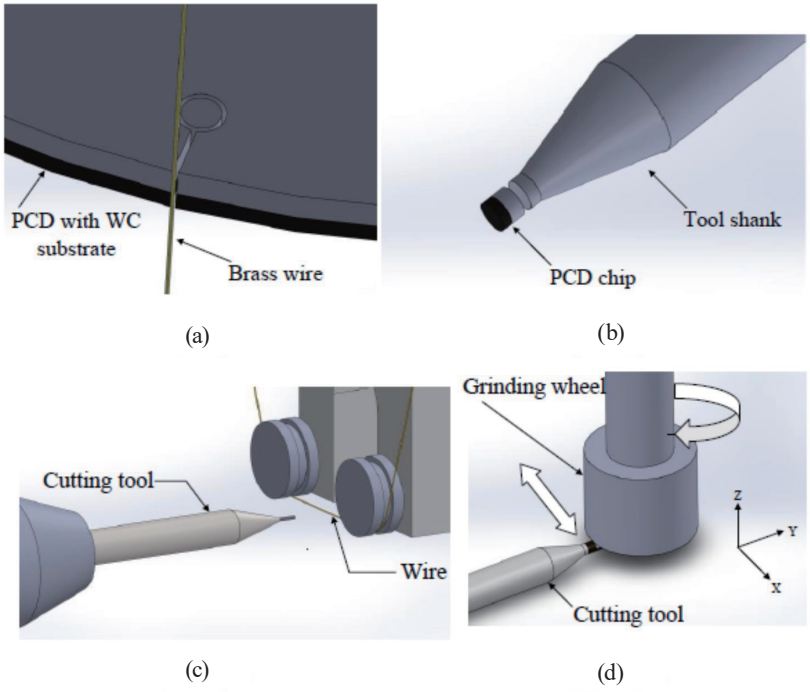

Fig. 2. (Color online) Schematic of manufacturing PCD cutting tools. (a) Step 1, (b) step 2, (c) step 3, and (d) step 4.

grinding wheels: electroplated and resin-bonded diamond grinding wheels. Both grinding wheels have a diameter of 10 mm and a height of 8 mm, with particle sizes of 20 and 15 μm, respectively. The machining parameters used in wire-EDM and abrasive grinding are listed in Table 2.

The microtools were assessed using a KEYENCE VHX-5000 optical microscope. A laser interferometer, ZYGO GPI-XP4, is preferred to conduct accurate surface inspection and measurement. The Raman spectrum of the BD-PCD surface was acquired using a laser Raman microspectroscopy apparatus, Nanofinder 30A. The objective of the Raman spectrum investigation was to examine the graphitization phenomenon in diamonds. Scanning electron microscopy (SEM) was utilized to obtain BD-PCD images to evaluate the material's surface integrity and edge quality.

Table 2
Machining parameters used in wire-EDM and abrasive grinding.

Item	Values
High-power source (V)	100
Low-power source (V)	45
Pulse on-time (ns)	700
Pulse off-time (μs)	4
Wire tension (gf)	300
Feed rate (mm/min)	0.006
Depth of cut (μm)	0.1–1.0
Grinding speed (m/s)	2.6–18.3
Table feed rate (mm/min)	30–50

3. Results and Discussion

3.1 Surface morphology and thermal damage management in BD-PCD

3.1.1 Thermally damaged layer and wire-EDM

Initially, the thermally damaged layer of BD-PCD produced by wire-EDM was detected and effectively managed to remain within acceptable ranges. Figure 3 illustrates the thermally damaged layer of BD-PCD resulting from wire-EDM manufacturing. It can be seen that the thickness of the thermally damaged layer is 12.6 μm. The isopulse generator used in this research offers pulse discrimination and real-time pulse control capabilities for individual sparks in accordance with the assessment of the spark gap condition. This prevents electrode wire breakage while enhancing the spark gap condition. By appropriately modifying the power configurations, it is possible to effectively manage the thermally damaged layer to less than 15 μm. This, in turn, reduces the duration required for the following abrasive grinding procedure.

3.1.2 Raman spectroscopy analysis

Figure 4 depicts the Raman spectra of two BD-PCD samples. One is BD-PCD after wire-EDM, and the other is BD-PCD after wire-EDM and abrasive grinding. The figure illustrates the BD-PCD after wire-EDM, revealing two distinct peaks at 1339 and 1594 cm^{-1}. According to the characteristics of the Raman spectrum, these peaks signify the presence of the diamond sp3 and graphite sp2 structures, respectively. During processing characterized by high temperatures, a diamond, consisting of carbon atoms bonded in an sp3 hybridization state, unavoidably transforms into graphite, wherein the carbon atoms are bonded in an sp2 hybridization state. The presence of two peaks in the red line can be attributed to this phenomenon. In contrast, the Raman spectrum of the BD-PCD sample acquired after wire-EDM and subsequent abrasive grinding reveals a distinct and pronounced peak at 1333 cm^{-1}, signifying the presence of only the sp3 diamond structure. The Raman spectroscopic analysis revealed that the surface graphitization of BD-PCD resulted from the thermal damage inflicted on the diamond during wire-EDM. The results revealed neither a residual graphite layer nor any newly formed on BD-PCD during the abrasive grinding.

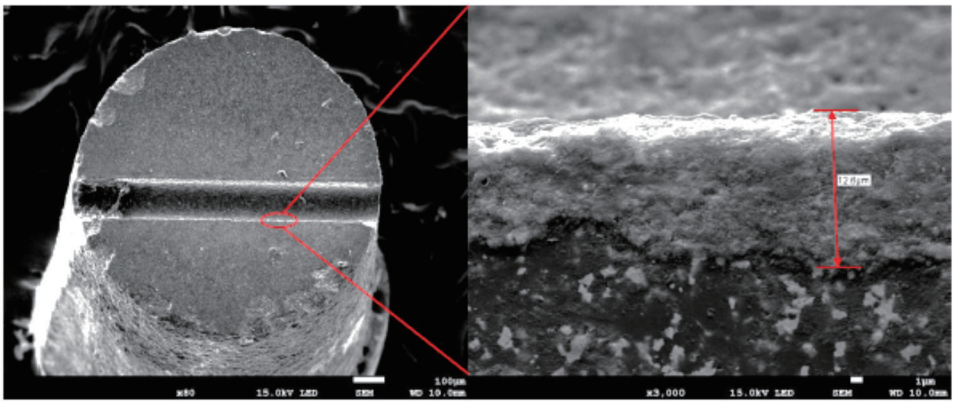

Fig. 3. (Color online) Thermally damaged layer of BD-PCD produced by wire-EDM.

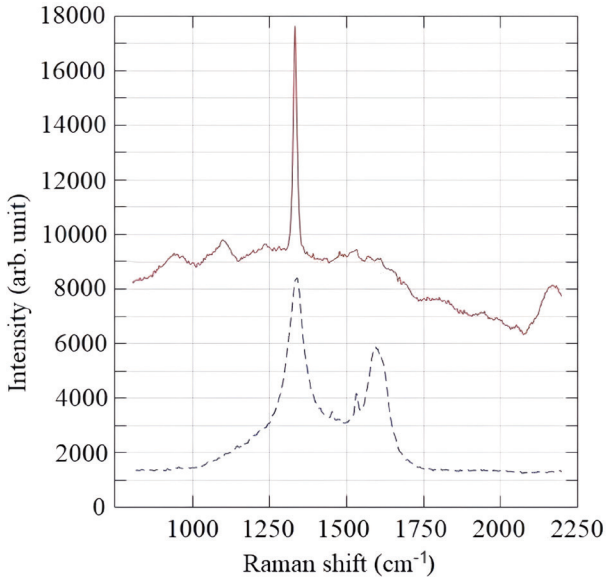

Fig. 4. (Color online) Raman spectra of BD-PCD after wire-EDM and BD-PCD after wire-EDM and abrasive grinding.

3.1.3 Surface integrity analysis and grinding wheel selection

To verify the material removal mechanism of BD-PCD with sequential wire-EDM and abrasive grinding, the surface integrity of the machined BD-PCD must be carefully evaluated. To facilitate the examination of the microscopic changes of the thermally damaged region pre- and post-wire-EDM, the measured grinding depth of 9.1 μm was employed for observation purposes. The depth of cut, grinding speed, and table feed rate were set as 0.1 μm, 18.3 m/s, and 30 mm/min, respectively. Figure 5 shows SEM images of the BD-PCD surface machined by different manufacturing processes. As shown in Fig. 5(a), the machined surface of BD-PCD exhibits many microdischarge craters and white debris particles adhering to the surface after wire-EDM. It can be seen from Fig. 5(b) that a thermally damaged layer of irregular form and

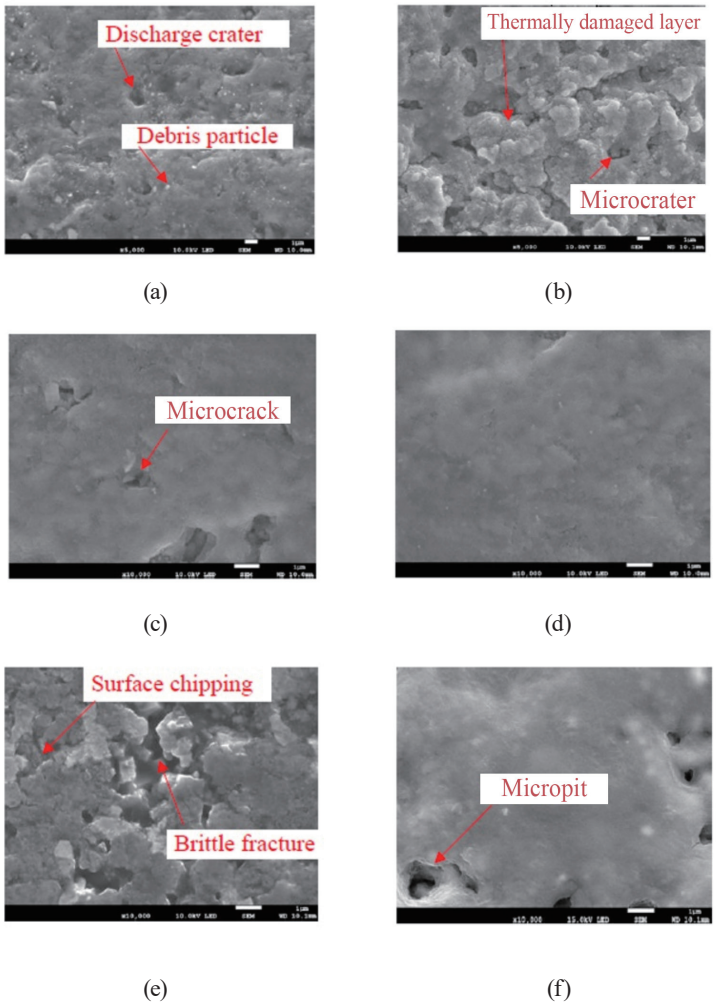

Fig. 5. (Color online) SEM images of the machined surface of BD-PCD. (a) Wire-EDM. (b) Sequential wire-EDM and abrasive grinding with electroplated diamond wheels; grinding depth < 9.1 μm. (c) Sequential wire-EDM and abrasive grinding with electroplated diamond wheels; grinding depth = 9.1 μm. (d) Sequential wire-EDM and abrasive grinding with resin-bonded diamond wheels; grinding depth = 9.1 μm. (e) Sequential wire-EDM and abrasive grinding with electroplated diamond wheels; grinding depth > 9.1 μm. (f) Sequential wire-EDM and abrasive grinding with resin-bonded diamond wheels; grinding depth > 9.1 μm.

many deep microdischarge craters appear on the machined surface of BD-PCD after sequential wire-EDM and abrasive grinding with electroplated diamond wheels when the grinding depth is less than the thickness of the thermally damaged layer. The presence of microdischarge craters and white debris particles on the machined surface of BD-PCD after abrasive grinding indicates that wire-EDM introduces significant damage to the surface of BD-PCD.

To thoroughly remove the thermally damaged layer and improve the surface integrity of BD-PCD, further modified grinding is necessary. In Fig. 5(c), the thermally damaged layer can be removed entirely by abrasive grinding with electroplated diamond wheels when the grinding depth is equal to the thickness of the thermally damaged layer. However, some microcracks are still observed on the surface of BD-PCD, indicating that the grinding process with electroplated

diamond wheels does not eliminate all forms of damage. The change of the grinding wheels to resin-bonded diamond wheels further reduced the surface damage, as shown in Fig. 5(d). By sequential wire-EDM and abrasive grinding with resin-bonded diamond wheels, we achieved a fracture-free surface with almost no apparent microcracks when the thermally damaged layer was removed entirely. Applying a resin-bonded diamond wheel verifies that a plastically deformed material removal process can grind the surface graphitic layer produced by wire-EDM without causing any further fracture cracks or damage under the surface.

To investigate the effects of different grinding wheels on the surface and subsurface damage of BD-PCD, the grinding process was continued beyond the thickness of the thermally damaged layer to examine possible subsurface damage. It can be seen from Fig. 5(e) that when the BD-PCD surface is ground with an electroplated diamond grinding wheel, brittle fracture and surface chipping occur on the processed BD-PCD surface. In contrast to the brittle fracture characteristics, Figure 5(f) shows that a smoother surface with some microcracks can be obtained when using a resin-bonded diamond wheel. When grinding BD-PCD, we found that the electroplated diamond grinding wheel exhibits superior bonding strength compared with the resin bond diamond grinding wheel. The diamond particles of the resin-bonded wheel easily fall out, exposing new diamond particles and cutting edges. In contrast, the diamond particles on the electroplated wheel demonstrate enhanced resistance to detachment during the grinding process. Therefore, as the grinding operation progresses, the diamond particles on the electroplated wheel gradually lose their sharpness, leading to increased brittle fractures and ultimately resulting in a rougher surface finish. The study results show that selecting the appropriate grinding wheel is crucial for achieving the desired surface and subsurface quality in the fabrication of BD-PCD cutting tools by combining wire-EDM and abrasive grinding. Applying a resin-bonded diamond grinding wheel resulted in a smooth surface of BD-PCD.

3.2 Effect of abrasive grinding parameters on edge integrity and surface quality

The attainment of high-quality BD-PCD cutting tools heavily relies on the optimization of cutting parameters. Specifically, essential parameters such as the depth of cut and grinding speed have been found to significantly affect the tools' maximum edge and surface chipping. Research has shown that increasing the depth of cut can lead to a rapid escalation of maximum edge chipping. At the same time, higher grinding speeds result in a decrease in grinding force, thereby reducing both maximum edge and surface chipping.[20,21] These findings emphasize the importance of carefully adjusting these parameters to attain the highest tool quality. Owing to the higher surface quality, only the microtools ground using the resin-bonded diamond grinding wheel are studied below. Figures 6(a) and 6(b) respectively show the edge and surface chipping of BD-PCD microtools with a cross-shaped cutting edge produced by abrasive grinding with a resin-bonded diamond wheel. Figure 7 illustrates the effect of varying the depth of cut on the occurrence of the maximum edge chipping. In this experimental setup, the grinding speed is constant at 13.1 m/s. There is an observed correlation between the depth of cut and the rate of increase in maximal edge chipping. Increasing the depth of cut yields a corresponding escalation in grinding force, consequently increasing the occurrence of the maximum edge chipping. When

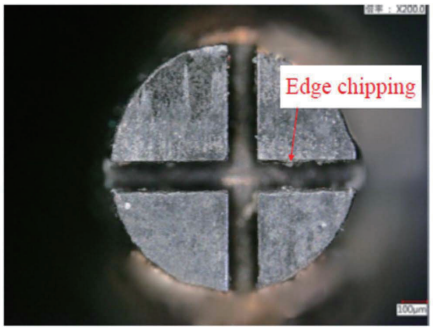

(a)

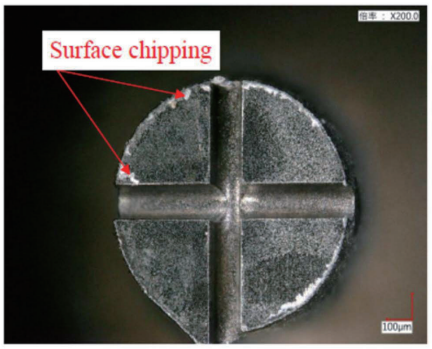

(b)

Fig. 6. (Color online) Edge and surface chipping of BD-PCD microtools with cross-shaped cutting edge produced by abrasive grinding with a resin-bonded diamond wheel. (a) Edge chipping. (b) Surface chipping.

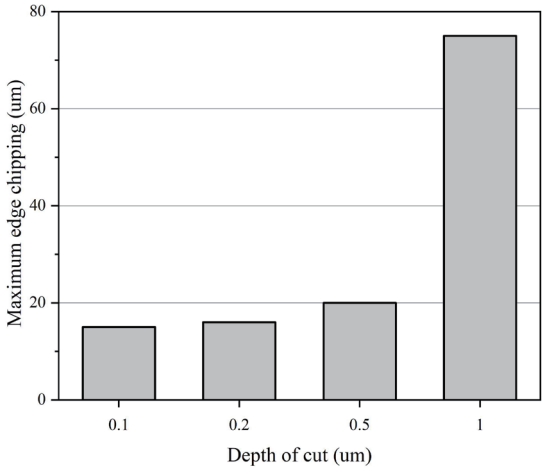

Fig. 7. Effect of depth of cut on maximum edge chipping.

the depth of cut is set to 0.1 μm, it is possible to achieve a maximum edge chipping of 13 μm. Figure 8 illustrates the impact of grinding speed on the occurrence of maximum surface chipping. Again, the depth of cut for this experiment is set at 0.1 μm. The results show a

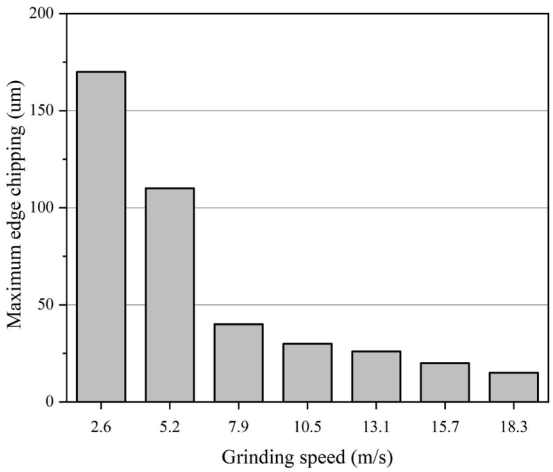

Fig. 8. Effect of grinding speed on maximum edge chipping.

significant decrease in maximum surface chipping as the grinding speed increases. As the grinding speed increases, the grinding power decreases, reducing the maximum surface chipping. It can be seen from Fig. 9 that a maximum surface chipping area of 1109 μm^2 is possible by setting the grinding speed to 18.3 m/s. Our findings indicate a clear relationship between grinding speed and grinding force, affecting the maximum edge and surface chipping. We observe a decrease in grinding pressure as the grinding speed increases. This decrease in grinding force ultimately leads to a decrease in maximum edge and surface chipping. This relationship among grinding speed, grinding force, and chipping highlights the importance of controlling the grinding parameters to achieve the desired outcomes. By adjusting the grinding speed and depth of cut, manufacturers can effectively minimize the occurrence of surface chipping during the grinding process. These results have practical implications for industries that rely on grinding operations, such as metalworking or manufacturing.

3.3 Evaluation of BD-PCD microcutting tools

After determining the optimal manufacturing parameters, the S-PCD and BD-PCD microtools were examined using SEM after undergoing sequential wire-EDM and abrasive grinding. Figure 10(a) shows the presence of edge chipping and microcracks on the cutting edge and flank face of the S-PCD microtool. As shown in Fig. 10(b), no edge chipping was observed on the cutting edge of the BD-PCD microtool. The BD-PCD microtool exhibited superior edge integrity and surface quality compared with the S-PCD tool because of its higher hardness and fracture toughness. Consequently, BD-PCD was more amenable to finishing using resin-bonded diamond wheels through abrasive grinding.

To evaluate the cutting efficacy of the BD-PCD microcutting tools produced, cutting experiments were conducted on BK7 glass. The designed microcutting tools can be classified into three categories on the basis of the manufacturing process employed. There are three tools, A, B, and C, produced using different manufacturing techniques. Tool A is manufactured using

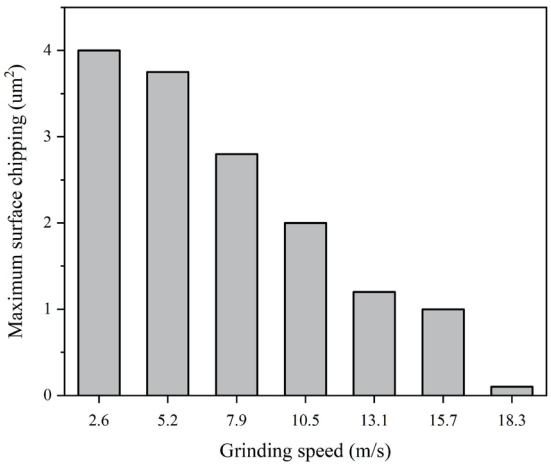

Fig. 9. Effect of grinding speed on maximum surface chipping.

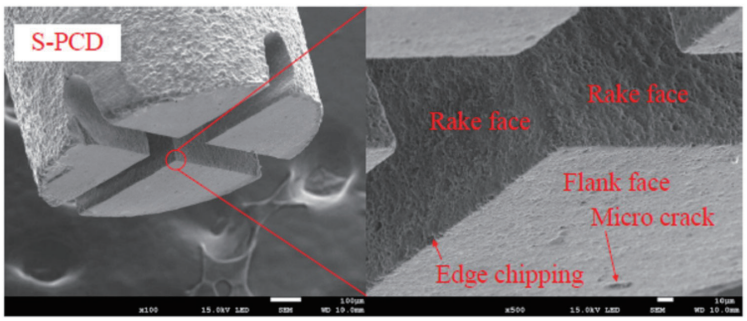

(a)

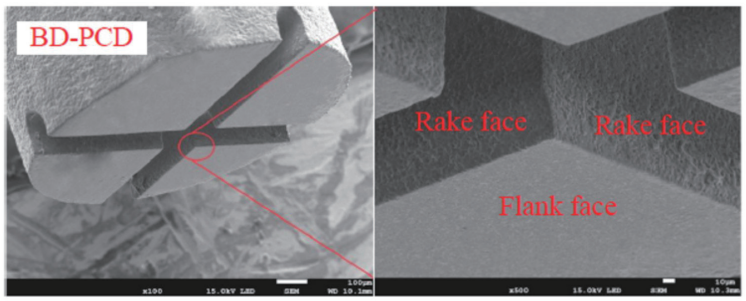

(b)

Fig. 10. (Color online) PCD microtools with cross-shaped cutting edge produced by sequential wire-EDM and abrasive grinding with a resin-bonded diamond wheel. (a) S-PCD tool and (b) BD-PCD tool.

wire-EDM, whereas, in the case of tool B, sequential wire-EDM and abrasive grinding with an electroplated diamond wheel are used. Tool C, on the other hand, is manufactured using sequential wire-EDM and abrasive grinding with a resin-bonded diamond wheel. The impact of various tools on the surface quality of BK7 glass was assessed and examined. Table 3 shows the

Table 3
Microgrinding performance characteristics of BD-PCD tools fabricated using different manufacturing processes.

Shape of cutting edge	Tool A	Tool B	Tool C
Sa (nm)	19	11	6

microgrinding effectiveness of the three types of BD-PCD grinding tools. Table 3 shows that all three BD-PCD grinding tools generate microcrack-free, nanoscale surfaces. A highly refined surface with a roughness of 6 nm Sa was possible using tool C. The study's findings revealed a positive correlation between the quality of the tool's cutting edge and the resulting surface roughness during the grinding of BK7 glass.

To investigate material accumulation around the grinding tools and analyze tool wear mechanisms in microgrinding, the tool wear patterns of two BD-PCD tools (tools B and C) were studied. After the grinding of optical BK7 glass, microscopic imaging was utilized to record and analyze the tool wear patterns exhibited by these tools. Microscopic images of two worn BD-PCD grinding tools are shown in Fig. 11. In Fig. 11(a), the microscopic image of tool B is shown. Again, this tool is manufactured using sequential wire-EDM and abrasive grinding employing an electroplated diamond wheel. The enlarged area in Fig. 11(a) reveals the presence of chips on the microgrooves of the grinding tool. Additionally, some chips have gathered and become attached to the flank face of tool B. Furthermore, a microcrater was formed on the lower edge of the flank face. Figure 11(b) shows the microscopic image of tool C, which has been produced through sequential wire-EDM and abrasive grinding employing a resin-bonded diamond wheel. An examination of Fig. 11(b) reveals the presence of abrasion wear on the right edge of the flank face and the occurrence of microchipping on the right periphery of tool C. The primary forms of wear observed in worn BD-PCD tools are classified as abrasion on the flank face and chipping on the perimeter of the grinding tool, as determined through morphological analysis. Concerning the abrasion observed on the flank face, note that the repetitive abrasion induced by silicon particles originating from the hard glass material during the rotational movement of the grinding tool might lead to the gradual wearing down of the outer region of the flank face. The abrasion on the flank face occurs owing to the separation of the metallic cobalt and boron-doped diamond grains caused by the breakage of the binders that join them. This separation leads to the movement of the diamond grains away from the BD-PCD surface. The occurrence of chipping along the periphery of BD-PCD tools can be attributed to the intermittent cutting load at high speeds during the machining of BK7 glass. This section encompasses the thorough examination and analysis of tool wear mechanisms in microgrinding. The results presented in this section form the foundation of the removal mechanism of BD-PCD when utilizing sequential wire-EDM and abrasive grinding.

3.4 Removal mechanism of BD-PCD material in sequential wire-EDM and abrasive grinding

Abrasive grinding is a machining technique wherein discrete abrasive grains are employed as cutting implements to eliminate chips effectively during the process. Hence, the overall grinding

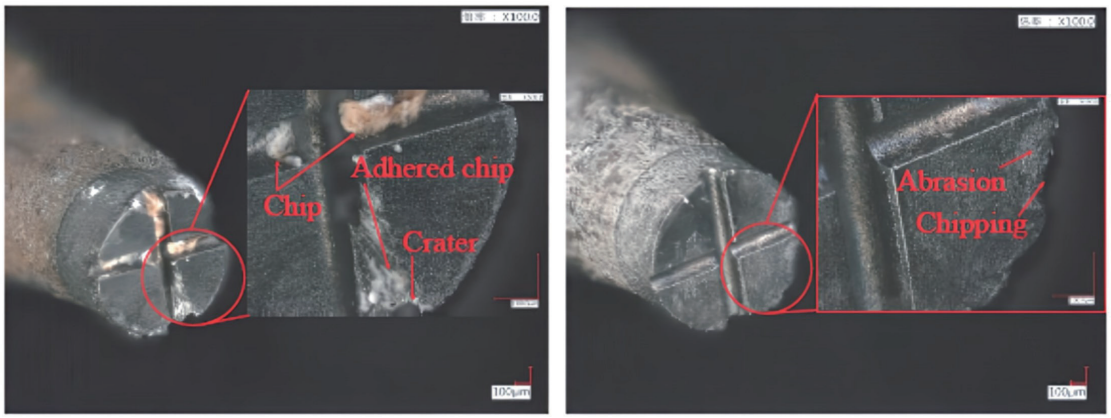

Fig. 11. (Color online) Microscopic images of two worn BD-PCD grinding tools: (a) tool B and (b) tool C both with cross-shaped cutting edge.

performance can be regarded as the cumulative outcome of the performance exhibited by each abrasive grain.[22] In this study, we propose a mechanism of the removal of material between a single abrasive diamond grain and BD-PCD, as illustrated in Fig. 12.

The initial stage involves the shaping of BD-PCD by wire-EDM. During this phase, electric discharge eliminates the conductive diamond particles in BD-PCD. This elimination is attributed to the electrical conductivity of the metallic cobalt and boron-doped diamond grains. The melting and vaporization of microdiamond particles during wire-EDM facilitate the cutting of conductive diamond grains through spark erosion, resulting in their limited susceptibility to detach from the BD-PCD surface. This stage is shown in Fig. 12(a).

The subsequent stage involves the development of a thermally damaged layer on the machined surface of BD-PCD. The spark erosion in wire-EDM generates numerous micropits and a thermally damaged layer on the machined surface of BD-PCD, as illustrated in Fig. 12(b). The generation of the thermally damaged layer is attributed to the elevated temperature and electric sparks involved in the process—an increase in discharge energy results in a thicker layer of thermal damage. The transition of the surface carbon structure of boron-doped diamond grains to graphite during wire-EDM is verified by examining Raman spectra. The findings align with those of prior research.[23,24]

The third stage is the removal of the thermally damaged layer. In previous research investigations, it was emphasized that, in cases where the grit depth of grinding falls below the critical uncut chip thickness, brittle materials can be removed through plastic flow, resulting in a surface free of cracks.[25,26] The critical uncut chip thickness (d_c), which is responsible for determining the transitions between brittle and ductile behaviors, was calculated by applying the mechanical parameters of the graphite material provided in Table 4 to Eq. (1).[27]

$$d_c = 0.15\left(\frac{E}{H}\right)\left(\frac{K_{IC}}{H}\right)^2 \tag{1}$$

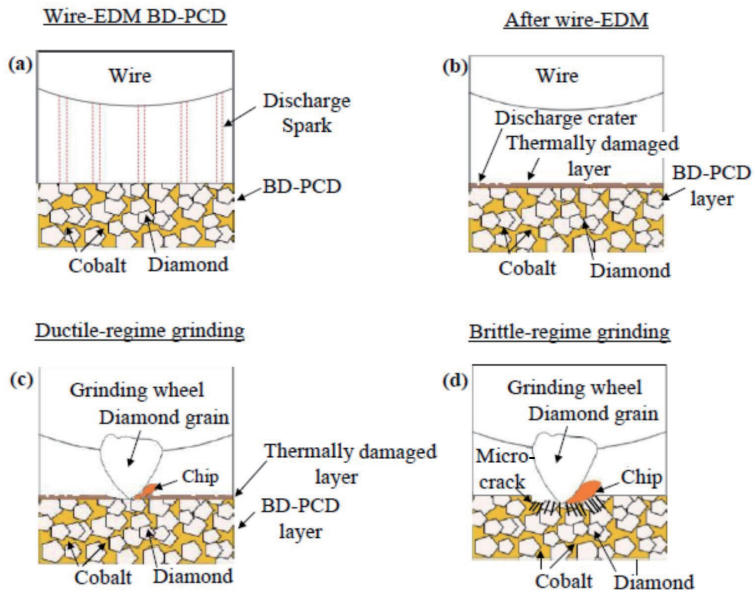

Fig. 12. (Color online) Material removal mechanism of BD-PCD with sequential wire-EDM and abrasive grinding.

Table 4
Mechanical properties of graphite material.

Property	Value
Young's modulus (GPa)	8.5–13
Hardness (MPa)	250
Fracture toughness (MPa$\sqrt{\text{m}}$)	2.2
Thermal conductivity (W/m·K)	200–300
Density (g/cm^3)	1.7

Here, E is Young's modulus of the material, H is the material hardness, and K_{IC} is the material fracture toughness.

Theoretical calculations yield a value of 395 μm for the critical uncut chip thickness in the graphite material. Theoretically, it is hypothesized that while the grit depth of grinding remains below 395 μm, the graphite material may be removed by a mechanism characterized by plastic flow rather than fracture. Hence, the above-mentioned procedure is considered to be ductile-regime or ductile-mode grinding. Figure 12(c) illustrates the removal of the thermally damaged layer generated by wire-EDM applying ductile-regime grinding. Given the specific machining conditions employed, it is possible to effectively eliminate materials while inhibiting the initiation of residual cracks beneath the surface. Consequently, the resulting surface is predominantly devoid of microcracks.

The fourth stage encompasses BD-PDB surface grinding. After the graphite layer is removed, the surface of BD-PCD experiences a continual cutting action of the diamond grains. On the basis of Eq. (1), it can be inferred that the critical uncut chip thickness necessary for BD-PC is around 0.044 μm. In contrast to the third stage, the fourth stage can be characterized as brittle-

regime grinding because the depth of grit surpasses 0.044 μm. Figure 12(d) illustrates the surface of BD-PCD after brittle-regime grinding. Using a diamond wheel for grinding PCD tools can result in undesirable effects such as microcracking, microgrooving, and edge chipping, exacerbated by a significant grit depth of grinding. The experimental data reported in the preceding sections validated the proposed material removal process.

4. Conclusions

In this study, we explored the complicated factors affecting the production of high-quality microcutting tools using BD-PCD. The manufacture of a tabletop machine tool was achieved using a specifically developed on-machine tool that combined sequential wire-EDM and abrasive grinding. Raman spectroscopy revealed how thermal deterioration affects material qualities owing to the conversion of diamond to graphite at high temperatures during manufacturing. The results of the surface integrity study indicated that surface damage can be controlled by selecting the appropriate grinding wheel. The impact of abrasive grinding parameters on the edge and surface quality was extensively studied, highlighting the importance of the depth of cut and grinding speed in reducing chipping. Microgrinding experiments confirmed the effectiveness of the fabricated BD-PCD cutting tools in cutting BK7 glass. The suggested material removal method, which includes shaping, thermally damaged layer removal, and grinding, provides a complete foundation for understanding the fabrication process. This study contributes to understanding the challenges of high-quality BD-PCD cutting tool manufacturing. It also offers practical suggestions for improving production processes and parameters. The study's findings underscore the importance of the precise parameter control of the surface quality, edge integrity, and performance of microcutting tools.

Acknowledgments

The authors would like to thank the National Science and Technology Council, which supported this work under grant no. MOST112-2622-E-167-003. The authors are also grateful to the Precision Instrument Support Center of Chia-Yi University.

References

1 L. Wondraczek, E. Bouchbinder, A. Ehrlicher, J. C. Mauro, R. Sajzew, and M. M. Smedskjaer: Adv. Mater. **34** (2022) 2109029. http://dx.doi.org/10.1002/adma.202109029
2 X. Wang, H. Guo, G. Wu, and S. Ding: Mater. Manuf. Processes **37** (2022) 1652. http://dx.doi.org/10.1080/10426914.2022.2032146
3 X. Wang, C. Li, H. Guo, G. Li, and S. Ding: Mater. Manuf. Processes **35** (2020) 449. http://dx.doi.org/10.1080/10426914.2020.1732413
4 P. Ong, C. H. Chong, M. Z. bin Rahim, W. K. Lee, C. K. Sia, and M. A. H. bin Ahmad: J. Intell. Manuf. **31** (2020) 227. http://dx.doi.org/10.1007/s10845-018-1443-6
5 S.-T. Chen, C.-H. Chen, and C.-H. Chang: Diamond Relat. Mater. **94** (2019) 155. http://dx.doi.org/10.1016/j.diamond.2019.03.010
6 S. N. B. Oliaei, Y. Karpat, J. P. Davim, and A. Perveen: J. Manuf. Processes **36** (2018) 496. http://dx.doi.org/10.1016/j.jmapro.2018.10.038
7 J. O'Hara and F. Fang: Int. J. Extreme Manuf. **1** (2019) 032003. http://dx.doi.org/10.1088/2631-7990/ab3e7f

8 S. N. B. Oliaei, C. Özdemir, and Y. Karpat: Int. J. Mechatron. Manuf. Syst. **7** (2014) 246. http://dx.doi.org/10.1504/ijmms.2014.067166
9 S. T. Chen and C. H. Chang: Appl. Mech. Mater. **217–219** (2012) 2167. http://dx.doi.org/10.4028/www.scientific.net/AMM.217-219.2167
10 W. Chen, S. Ninomiya, S. Nochi, M. Iwai, and K. Suzuki: Adv. Mater. Res. **1017** (2014) 770. http://dx.doi.org/10.4028/www.scientific.net/AMR.1017.770
11 M.-T. Yan and T.-C. Lin: Procedia CIRP **42** (2016) 709. http://dx.doi.org/10.1016/j.procir.2016.02.306
12 X. Cheng, K. Nakamoto, M. Sugai, S. Matsumoto, Z. G. Wang, and K. Yamazaki: CIRP Annals **57** (2008) 415. http://dx.doi.org/10.1016/j.cirp.2008.03.137
13 X. Cheng, Z. Wang, K. Nakamoto, and K. Yamazaki: J. Mech. Sci. Technol. **24** (2010) 2261. http://dx.doi.org/10.1007/s12206-010-0804-7
14 A. Pratap, K. Patra, and A. A. Dyakonov: Int. J. Adv. Manuf. Technol. **104** (2019) 63. http://dx.doi.org/10.1007/s00170-019-03831-x
15 C. Morgan, R. R. Vallance, and E. R. Marsh: Proc. 20th Annual ASPE Meeting, ASPE 2005 (2005). https://www.scopus.com/inward/record.uri?eid=2-s2.0-84884870005&partnerID=40&md5=7d90b651b46ec7faa3f6e1786761839b
16 T. Schaller, L. Bohn, J. Mayer, and K. Schubert: Precis. Eng. **23** (1999) 229. http://dx.doi.org/10.1016/S0141-6359(99)00011-2
17 J. C. Aurich, I. G. Reichenbach, and G. M. Schüler: CIRP Annals **61** (2012) 83. http://dx.doi.org/10.1016/j.cirp.2012.03.012
18 Z. Zhan, L. Li, N. He, and R. Shrestha: Int. J. Adv. Manuf. Technol. **73** (2014) 1799. http://dx.doi.org/10.1007/s00170-014-5969-2
19 G. Li, M. Z. B. Rahim, S. Yi, S. Ding, S. Sun, J. Mo, and M. Rahman: Mater. Today Proc. **4** (2017) 5248. http://dx.doi.org/10.1016/j.matpr.2017.05.034
20 A. Pratap, K. Patra, and S. S. Joshi: J. Manuf. Sci. Eng. **145** (2023) 041007. http://dx.doi.org/10.1115/1.4056490
21 A. Perveen, W. Y. San, and M. Rahman: Int. J. Adv. Manuf. Technol. **61** (2012) 101. http://dx.doi.org/10.1007/s00170-011-3688-5
22 X. Chen and W. B. Rowe: Int. J. Mach. Tools Manuf. **36** (1996) 883. http://dx.doi.org/10.1016/0890-6955(96)00117-4
23 S.-T. Chen and C.-H. Chang: J. Mater. Process. Technol. **213** (2013) 740. http://dx.doi.org/10.1016/j.jmatprotec.2012.11.027
24 M.-T. Yan, Y.-C. Cheng, and S.-Y. Luo: Int. J. Precis. Eng. Manuf. **20** (2019) 159. http://dx.doi.org/10.1007/s12541-019-00052-w
25 E. K. Antwi, K. Liu, and H. Wang: Front. Mech. Eng. **13** (2018) 251. http://dx.doi.org/10.1007/s11465-018-0504-z
26 W. K. Neo, A. S. Kumar, and M. Rahman: Int. J. Adv. Manuf. Technol. **63** (2012) 465. http://dx.doi.org/10.1007/s00170-012-3949-y
27 T. G. Bifano, T. A. Dow, and R. O. Scattergood: J. Eng. Ind. **113** (1991) 184. http://dx.doi.org/10.1115/1.2899676

About the Authors

Yue-Feng Lin received his B.S., M.S., and Ph.D. degrees from National Cheng Kung University, Taiwan, in 2008, 2009, and 2016, respectively. From 2017 to 2018, he was a postdoctoral researcher at National Chung Hsing University, Taiwan. Since 2018, he has been an assistant professor at National Chin-Yi University of Technology, Taiwan. His main research areas include the application of ultrasonic-vibration-assisted nontraditional processing methods to ceramic, hard, and brittle materials. (yflin@ncut.edu.tw)

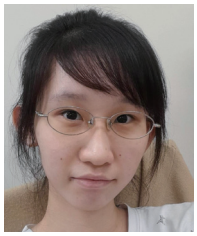

Pei-Yu Lai received her B.S. and M.S. degrees from National Chin-Yi University of Technology, Taiwan, in 2021 and 2022, respectively. Her main research areas include carbon emission, process capability analysis, process quality, and statistical testing. (ncut3a615182@gmail.com)

Yuan-Xiu Luo received his B.S. and M.S. degrees from National Chin-Yi University of Technology, Taiwan, in 2021 and 2023, respectively.